Structural properties and optical response of Na clusters in Ne, Ar, and Kr matrices

F. Fehrer
Institut für Theoretische Physik, Universität Erlangen, Staudtstrasse 7, D-91058 Erlangen, Germany

P. M. Dinh and E. Suraud
Laboratoire de Physique Théorique, IRSAMC, CNRS, Université de Toulouse, 118 route de Narbonne, F-31062 Toulouse Cédex, France

P.-G. Reinhard
Institut für Theoretische Physik, Universität Erlangen, Staudtstrasse 7, D-91058 Erlangen, Germany and Laboratoire de Physique Théorique, IRSAMC, CNRS, Université de Toulouse, 118 route de Narbonne, F-31062 Toulouse Cédex, France

(Received 24 October 2006; revised manuscript received 19 April 2007; published 14 June 2007)

We discuss the structural properties and optical response of a small Na cluster inside rare-gas (RG) matrices of Ne, Ar, or Kr atoms. The mixed systems are described with a hierarchical model, treating the cluster at a quantum-mechanical level and the matrix atoms classically in terms of their positions and polarizations. We pay special attention to the differences caused by the different matrix types. These differences can be explained by the interplay of core repulsion and dipole attraction in the interaction between the cluster electrons and the RG atoms.

DOI: 10.1103/PhysRevB.75.235418 PACS number(s): 36.40.Gk, 36.40.Jn, 36.40.Qv, 36.40.Sx

I. INTRODUCTION

The study of the properties of clusters embedded in a matrix or deposited on a substrate has motivated many researches for several years.[1,2] This setup becomes increasingly important because embedding and/or depositing simplifies the experimental handling and because it is a generic test case for composite materials. As in free clusters, the doorway to (laser induced) cluster dynamics is the optical response, especially in metal clusters where the Mie plasmon dominates the optical properties.[3] Let us mention as examples the systematics of optical response in large noble-metal clusters[4–7] and its dependence on the environment.[8] The study of the optical response thus constitutes the key for understanding the response of clusters to electromagnetic probes and it also serves as a powerful tool for analyzing the underlying cluster structure.

The case of inert environments is especially interesting because it implies only moderate perturbations of cluster properties. One can thus benefit from the well-defined conditions from the surrounding system and still access predominantly the cluster properties. But the theoretical modeling becomes much more involved and the development of reliable as well as inexpensive approaches is still a timely task, in particular, which truly dynamical applications are concerned.[9–11] Nonetheless, fully detailed calculations have been undertaken where details count, e.g., for the structure of small Na clusters on NaCl (Ref. 12) or the deposit dynamics of Pd clusters on a MgO substrate.[13] However, the expense for a fully fledged quantum simulation grows huge. These subtle models are hardly extendable to truly dynamical situations, to larger clusters or substrates, and to systematic explorations for broad variations of conditions. This holds true not only for clusters on substrates, but for all composite systems. Thus there exists a great manifold of approximations which aim at an affordable compromise between reliability and expense. One route, for example, keeps all constituents at the same level, but simplifies the description in terms of a microscopically founded tight-binding approach.[14–19] At the other extreme, one can consider all degrees of freedom as classical and perform pure molecular dynamics, as, e.g., the deposition dynamics of Cu clusters on metal[20] or Ar (Ref. 21) surface, and of Al or Au clusters on SiO_2.[22] In between, one can take advantage of the very different importance or activity within the composite, and thus, develop a hierarchical modeling using various levels of approximation for the different subsystems. Such approaches are widely used in quantum chemistry, often called quantum-mechanical–molecular-mechanical (QM/MM) model. They have been applied, for instance, to chromophores in biomolecules,[23,24] surface physics,[25,26] materials physics,[27–30] embedded molecules,[31] and ion channels of cell membranes.[32] A variant of mixed modeling was applied in the case of a Cs atom in He environment; the latter also considered as a quantum system.[33]

We are dealing here with Na clusters in rare-gas environments (Ne, Ar, and Kr). The large difference between cluster metals (reactive) and rare gas (inert) naturally suggests a hierarchical model, where the substrate atoms are handled at a lower level of description, as classical particles but with a dynamical polarizability. Taking up previous developments from Refs. 34 and 35, we have developed, in the spirit of QM/MM approaches, a hierarchical model for Na clusters in contact with Ar (Ref. 36) and applied it to structure and optical response[37] and to nonlinear dynamics of embedded clusters.[38] It is the aim of this paper to present a generalization to other types of rare gases (RGs), namely, Kr and Ne, and a comparative study of the effects of different environments on structure and optical response. As test cases, we consider a Na_8 cluster embedded in RG clusters of various sizes. Strictly speaking, they are mixed clusters, and properties which depend on the size of the RG system are specific to mixed clusters. However, we use the mixed systems mainly as model for Na clusters embedded in a matrix and

we thus consider rather large systems. Henceforth, we will use the notion "matrix" for the RG surroundings.

II. MODEL

The model has been introduced and presented in detail in Ref. 39. However, for the sake of completeness, we recall in this section the ingredients and a few relevant formulas.

The degrees of freedom of the model are the wave functions of valence electrons of the metal cluster, $\{\varphi_n(\mathbf{r}), n=1,\ldots,N_{\mathrm{el}}\}$, the coordinates of the cluster's Na^+ ion cores, $\{\mathbf{R}_I, I=1,\ldots,N_{\mathrm{ion}}\}$, of the Ar atoms cores Ar^{Q+}, $\{\mathbf{R}_a, a=1,\ldots,N_{\mathrm{Ar}}\}$, and of the Ar valence clouds, $\{\mathbf{R}'_a, a=1,\ldots,N_{\mathrm{Ar}}\}$. From the given total energy, the corresponding equations of motion are derived in a standard manner by variation. This leads to the (time-dependent) Kohn-Sham equations for the single-particle wave functions $\varphi_n(\mathbf{r})$ of the cluster electrons and Hamiltonian equations of motion for the other three degrees of freedom, thus treated by classical molecular dynamics (MD). For the valence cluster electrons, we use a density-functional theory at the level of the time-dependent local-density approximation (TDLDA), augmented with an average-density self-interaction correction (ADSIC).[40] The density of these electrons is given naturally as defined in mean-field theories and reads $\rho_{\mathrm{el}}(\mathbf{r}) = \Sigma_n |\varphi_n(\mathbf{r})|^2$. A RG atom is described by two constituents with opposite charge, positive RG core and negative RG valence cloud, which allows a correct description of polarization dynamics. In order to avoid singularities, we associate a smooth (Gaussian) charge distribution to both constituents having width σ_{RG} of the order of the p shell "size" in RG atoms, in the spirit of Ref. 34:

$$\rho_{\mathrm{RG},a}(\mathbf{r}) = \frac{eQ}{\pi^{3/2}\sigma_{\mathrm{RG}}^3}\left\{\exp\left[-\frac{(\mathbf{r}-\mathbf{R}_a)^2}{\sigma_{\mathrm{Ar}}^2}\right] - \exp\left[-\frac{(\mathbf{r}-\mathbf{R}'_a)^2}{\sigma_{\mathrm{Ar}}^2}\right]\right\}. \tag{1}$$

The corresponding Coulomb potential exerted by the RG atoms is related to the charge distribution (1) by the Poisson equation and reads

$$V^{(\mathrm{pol})}_{\mathrm{RG},a}(\mathbf{r}) = e^2 Q\left[\frac{\mathrm{erf}(|\mathbf{r}-\mathbf{R}_a|/\sigma_{\mathrm{RG}})}{|\mathbf{r}-\mathbf{R}_a|} - \frac{\mathrm{erf}(|\mathbf{r}-\mathbf{R}'_a|/\sigma_{\mathrm{RG}})}{|\mathbf{r}-\mathbf{R}'_a|}\right], \tag{2}$$

where $\mathrm{erf}(r) = \frac{2}{\sqrt{\pi}}\int_0^r dx e^{-x^2}$ stands for the error function. As for the Na^+ ions, their dynamical polarizability is neglected and we treat them simply as charged point particles.

The total energy of the system is composed as

$$E_{\mathrm{total}} = E_{\mathrm{Na\ cluster}} + E_{\mathrm{RG}} + E_{\mathrm{coupl}} + E_{\mathrm{VdW}}. \tag{3}$$

The energy of the Na cluster $E_{\mathrm{Na\ cluster}}$ consists of TDLDA (with SIC) for the electrons, MD for ions, and a coupling of both by soft, local pseudopotentials; for details see Refs. 11, 41, and 42. The RG system and its coupling to the cluster are described by

$$E_{\mathrm{RG}} = \sum_a \frac{\mathbf{P}_a^2}{2M_{\mathrm{RG}}} + \sum_a \frac{\mathbf{P}_a'^2}{2m_{\mathrm{RG}}} + \frac{1}{2}k_{\mathrm{RG}}(\mathbf{R}'_a - \mathbf{R}_a)^2 + \sum_{a<a'}\left[\int d\mathbf{r}\rho_{\mathrm{RG},a}(\mathbf{r})V^{(\mathrm{pol})}_{\mathrm{RG},a'}(\mathbf{r}) + V^{(\mathrm{core})}_{\mathrm{RG,RG}}(\mathbf{R}_a - \mathbf{R}_{a'})\right], \tag{4}$$

$$E_{\mathrm{coupl}} = \sum_{I,a}[V^{(\mathrm{pol})}_{\mathrm{RG},a}(\mathbf{R}_I) + V'_{\mathrm{Na,RG}}(\mathbf{R}_I - \mathbf{R}_a)] + \int d\mathbf{r}\rho_{\mathrm{el}}(\mathbf{r})\sum_a [V^{(\mathrm{pol})}_{\mathrm{RG},a}(\mathbf{r}) + W_{\mathrm{el,RG}}(|\mathbf{r}-\mathbf{R}_a|)], \tag{5}$$

$$E_{\mathrm{VdW}} = \frac{e^2}{2}\sum_a \alpha_a\left\{\frac{\left[\int d\mathbf{r}\mathbf{f}_a(\mathbf{r})\rho_{\mathrm{el}}(\mathbf{r})\right]^2}{N_{\mathrm{el}}} - \int d\mathbf{r}\mathbf{f}_a(\mathbf{r})^2\rho_{\mathrm{el}}(\mathbf{r})\right\} \quad \text{where } \mathbf{f}_a(\mathbf{r}) = \nabla\frac{\mathrm{erf}(|\mathbf{r}-\mathbf{R}_a|/\sigma_{\mathrm{RG}})}{|\mathbf{r}-\mathbf{R}_a|}. \tag{6}$$

The van der Waals interaction between cluster electrons and RG dipoles is written in Eq. (6) as a correlation from the dipole excitation in the RG atom coupled with a dipole excitation in the cluster, using the regularized dipole operator $\mathbf{f}_a$ corresponding to the smoothened RG charge distributions.[35,39]

The interaction of one RG atom with the other constituents (RG atoms, Na^+ ions, and cluster electrons) results from the balance between a strong repulsive core potential that falls off exponentially and an equally strong attraction from dipole polarizability. The (most important) polarization potential is described by a valence electron cloud oscillating against the RG core ion. Its parameters are the effective charge of valence cloud Q, the effective mass of valence cloud $m_{\mathrm{Ar}}=Qm_{\mathrm{el}}$, the restoring force for dipoles k_{RG}, and the width of the core and valence clouds σ_{RG}. The Q and k_{RG} are adjusted to reproduce experimental data on dynamical polarizability $\alpha_D(\omega)$ of the RG atom at low frequencies, namely, the static limit $\alpha_D(\omega=0)$ and the second derivative of $\alpha''_D(\omega''=0)$. The width σ_{RG} is determined consistently such that the restoring force from the folded Coulomb force (for small displacements) reproduces the spring constant k_{RG}.

The short-range repulsion is provided by the various core potentials. For the RG-RG core interaction in Eq. (4), we employ a Lennard-Jones-type potential with parameters reproducing binding properties of bulk RG:

$$V^{(\mathrm{core})}_{\mathrm{RG,RG}}(R) = e^2 A_{\mathrm{RG}}[(R_{\mathrm{RG}}/R)^{12} - (R_{\mathrm{RG}}/R)^6]. \tag{7}$$

The Na-RG core potential $V'_{\mathrm{Na,RG}}$ in Eq. (5) is chosen according to Ref. 43 properly avoiding double counting of the dipole polarization potential, hence the following form:

TABLE I. Properties of the RG atoms and Na-RG dimers for Ne, Ar, and Kr which were used for the fine tuning of the model.

	RG atom		Na-RG		RG bulk	
RG	α_{RG} (a_0^{-3})	IP (Ry)	d_0 (a_0)	E_0 (mRy)	r_s (a_0)	E_{coh} (mRy)
Ne	2.67	1.585	10.01	0.0746	5.915	−0.0272
Ar	11.08	1.158	9.47	0.3793	7.086	−0.1088
Kr	16.79	1.029	9.29	0.6238	7.540	−0.1497

$$V'_{\mathrm{Na,RG}}(R) = e^2\left[A_{\mathrm{Na}}\frac{e^{-\beta_{\mathrm{Na}}R}}{R} - \frac{2}{1+e^{\alpha_{\mathrm{Na}}/R}}\left(\frac{\alpha_{\mathrm{RG}}}{2R^4} + \frac{C_{\mathrm{Na},6}}{R^6} + \frac{C_{\mathrm{Na},8}}{R^8}\right)\right] + e^2\frac{\alpha_{\mathrm{RG}}}{2R^3}\mathbf{R}\cdot\nabla_{\mathbf{R}}\frac{\mathrm{erf}(R/\sqrt{2}\sigma_{\mathrm{RG}})}{R}. \tag{8}$$

The parameters are taken from literature for Na-Ne,[44] Na-Ar,[43,45] and Na-Kr.[46] The pseudopotential $W_{\mathrm{el,RG}}$ in Eq. (5) for the electron-RG core repulsion has been modeled according to the proposal of Ref. 34:

$$W_{\mathrm{el,RG}}(r) = e^2\frac{A_{\mathrm{el}}}{1+e^{\beta_{\mathrm{el}}(r-r_{\mathrm{el}})}}, \tag{9}$$

with a final slight adjustment to the properties of a Na-RG molecule (bond length, binding energy, and optical excitation spectrum). Values of atomic and dimer properties used are reported in Table I.

III. MODUS OPERANDI

The numerical solution proceeds with standard methods as described in detail in Ref. 42 The TDLDA equations for the cluster electrons are solved on a grid in coordinate space, using a time-splitting method for the propagation and accelerated gradient iterations for the stationary solution. We, furthermore, employ the cylindrically averaged pseudopotential scheme (CAPS) as an approximation for the electrons,[47,48] which is justified for the chosen embedded Na_8 cluster. We have checked that a two-dimensional calculation with CAPS and a full three-dimensional treatment of the valence electron wave functions both give almost identical optical responses. The Na^+ ions as well as the RG atoms are treated in full three dimensions. The dynamics of the Na electrons is coupled to the response of the RG dipoles. However, the ionic and atomic positions can safely be frozen for the present study as we focus on exploring the optical response of the embedded clusters.

To find an optimal Na+RG configuration, one starts with a fcc RG crystal, cuts from that a given number of closed shells, and cools the resulting configuration for a pure RG cluster. One then carves a cavity of 13 atoms (Ar and Kr) or 19 atoms (Ne) from the center and places the Na_8 cluster into it. This mixed configuration is reoptimized by means of successively cooled molecular dynamics for the ions and atoms coupled to the stationary solution for the cluster electrons.

The stationary solution of the equations of motion provides the ground state of the mixed system and constitutes the initial condition for further dynamical calculations. One can then compute several observables to analyze both the statics (structural properties) and the dynamics. A global measure for ionic and electronic cluster structures are the rms radii,

$$r_{I,e} = \sqrt{\langle(x^2+y^2+z^2)\rangle_{I,e}}, \tag{10}$$

where $\langle\ldots\rangle_I = \Sigma_I\ldots$ and $\langle\ldots\rangle_e = \int d^3\mathbf{r}\rho_e(\mathbf{r})\ldots$. Note that these quantities may also be used for characterizing dynamics, although they take interest mostly on very long times when ions and atoms actually move. This latter aspect is not directly addressed here and we shall thus use them only as static quantities. We also evaluate the insertion energy E_{ins}, which is defined as

$$E_{\mathrm{ins}} = E_{\mathrm{tot}}(\mathrm{Na_8RG}_N) + E(\mathrm{RG}_p) - E(\mathrm{RG}_{N+p}) - E(\mathrm{Na_8}), \tag{11}$$

with $p=13$ in the case of Ar and Kr, and $p=19$ for Ne. A further useful energetic observable is the ionization potential (IP), that is, the energy required to remove one electron from the metal cluster. We compute it as the single-particle energy of the least-bound electron, which is a reliable measure in ADSIC.[40]

At the side of truly dynamical properties, as already emphasized, one should recall the especially important role played by the optical response. This observable is computed in an explicitly dynamical way. The dynamics is initiated by an instantaneous dipole boost of the cluster electrons. The optical response is then obtained by spectral analysis of the emerging time-dependent dipole signal following the strategy proposed in Refs. 49–51

IV. RESULTS AND DISCUSSION

Figure 1 shows the RG structure in terms of radial distributions of atoms. The effect of embedding is visualized by comparing the pure RG system (dotted) with the RG distribution around the Na_8 cluster (full lines). The distributions line up nicely in radial shells. For pure RG clusters, they remain very close to the radial shells of the bulk fcc structure (not shown here; for the case of Ar, see Ref. 37). The overall scale is basically given by the bulk Wigner-Seitz radius r_s given in Table I. Note that Ne has a much smaller r_s, resulting in denser packing as seen in Fig. 1. Carving of the cavity and insertion of Na_8 only have a small effect on the Ar and Kr environments and mainly for a few inner shells. For Ne, however, we see a stronger perturbation which spreads over all atoms. The examples in Fig. 1 concern rather larger RG systems probably close to the bulk. The embedding effects increase with decreasing number of RG shells, remaining small throughout for Kr and Ar, but soon destroying any clear shell structure for Ne.[52] The reason is that Ne is much less bound than Ar or Kr as can be read off from the cohesion energy in Table I, and already these seemingly more robust materials are weakly bound.

The impact of the RG environment on metal cluster properties is analyzed in Fig. 2, which shows global observables

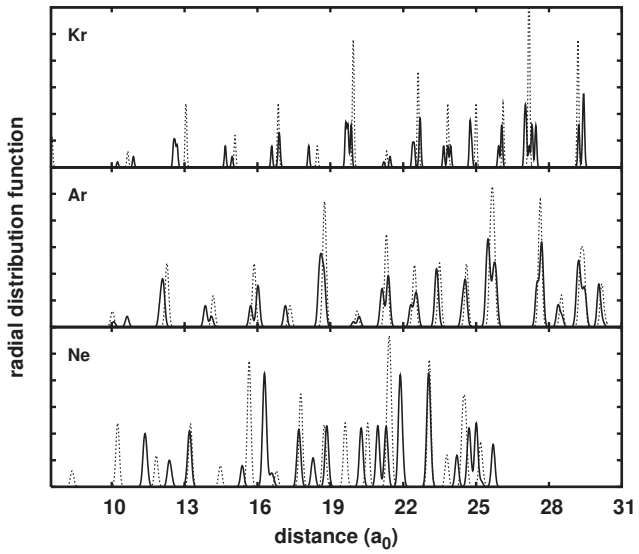

FIG. 1. Radial distribution of RG atoms in Na_8Ne_{428}, Na_8Ar_{434}, and Na_8Kr_{434} (full lines) compared with the distributions for the pure RG cluster with 447 atoms before carving the cavity (dashed lines).

of the ground-state configurations of Na_8 in the various matrices as a function of matrix size. The insertion energies in the uppermost panel indicate that Ne cannot finally capture Na_8 inside, while Ar, and even more so Kr, provides robust environments for embedded metal clusters. The binding increases slowly with matrix size, except for Ne where the polarizability is too weak to accumulate sufficient long-range attraction. The IP (second row in Fig. 2) makes a jump down from free Na_8 to the embedded cases and then stabilizes with a few fluctuations for small matrices and a faint further decrease for larger ones. The energies are at the same scale for all RG types. The sudden drop from free to embedded for Ar and Kr is due to the core repulsion from the first RG shell exerted on the cluster electrons. Adding further shells affects the cluster only indirectly by compressing the whole matrix

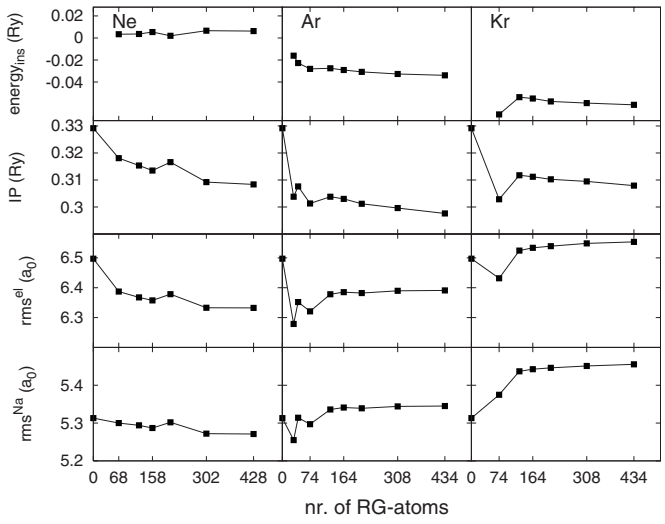

FIG. 2. Ground-state observables (energies and radii) for Na_8 embedded in Ne, Ar, and Kr matrices of different sizes.

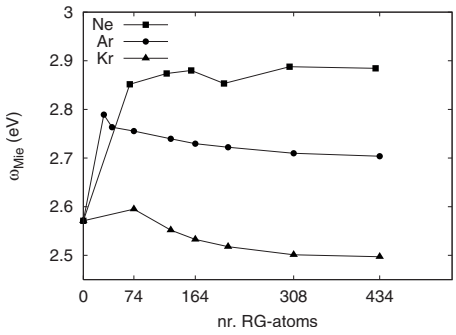

FIG. 3. Plasmon resonance energies for Na_8 in matrices of different sizes and RG materials.

and thus bringing the innermost shell slightly closer to the cluster. Radii in Na_8 are shown in the two lower rows. They vary very little in general. There remain interesting differences in detail. The trends with matrix size are the same for electrons and ions. However, the step from free to embedded is much different to the extent that electrons are more compressed when embedded, which is a visible effect from core repulsion, similar to the jump in IP. The radii decrease slightly with matrix size for Ne and increase for Ar or Kr. This indicates that core repulsion prevails in Ne, while dipole attraction becomes more effective in Ar and Kr.

We finally present in Fig. 3 the trends of the Na_8 plasmon resonance peak. The changes are generally small, at an absolute scale at the limits of our modeling (which we estimate to be about 0.1 eV uncertain). The relative trends, however, can be taken at smaller energy scale, and these carry several interesting aspects. As previously discussed,[37] the position of the peak results from a subtle cancellation between core repulsion and polarization effects. The step from free to embedded clusters first produces a blueshift because the cluster electrons feel the core repulsion from the first layer of RG atoms. The plasmon peak moves slowly back to red with increasing system size, because each new RG shell adds to the long-range and attractive polarization potential. Polarizability is also the key to the trend with RG material. It increases with atomic number (see column 2 of Table I). The cancellation mentioned above is thus more effective in Kr than in Ar, and in Ar more than in Ne. This explains the steady decrease of the peak position from Ne to Kr and the growth of slope with atomic number. In fact, Ne shows no significant slope to red at all. This happens because added atoms compress slightly the innermost shell (see shrinking radii with increasing system size in Fig. 2) and enhance core repulsion, which, in turn, compensates the growth of polarization effects. Ar and Kr experience no such compression and have, anyway, the stronger polarizability.

Experimental data for Na clusters embedded in rare-gas material are not yet available. A direct comparison, thus, has to be postponed. But there exist already some data on the optical response in the somehow similar combination of Ag clusters in RG material: the Lausanne group studied, among others, $Ag_8@Ar$,[53] $Ag_7@Ar,Kr,Xe$,[54] and $Ag_7@Ar,Ne$ (Ref. 55) in large RG matrices and, the Rostock group studied Ag_8 covered by small layers of Ne, Ar, Kr, and Xe (of sizes between 4 and 135 RG atoms) all immersed in a He droplet.[8]

TABLE II. Shift of plasmon peak position, in eV, going from one environment to another, as indicated. A plus (minus) sign stands for a blueshift (redshift).

Ag_7@		Ag_8@	
Ref. 55	Ref. 54	Ref. 53	Ref. 8
			$He_{drop} \rightarrow Ne_{135}$: 0.009
Ne → Ar: −0.1			
		$He_{drop} \rightarrow Ar$: −0.03	$He_{drop} \rightarrow Ar_{24}$: −0.01
	Ar → Kr: −0.06/−0.09		
			$He_{drop} \rightarrow Kr_{25}$: −0.04
			$He_{drop} \rightarrow Xe_{15}$: −0.08

Table II summarizes the results in terms of shifts of the plasmon peak position with changing RG material. A direct comparison with free neutral Ag clusters is not available because these are hard to handle experimentally. As for experiments performed in Ref. 8, Ag_8 is embedded in very small RG matrices, and the whole system itself embedded in a He droplet, for reasons of better handling. It is usually claimed that the helium environment interacts very faintly with the embedded system and can then be considered practically as a vacuum. However, experimental data[56,57] and density-functional theory calculations[33] show that the presence of He around Cs atoms produces a blueshift of the plasmon peak. It is thus likely that some small blueshift exists also for Ag clusters directly in He droplets. Therefore a comparison with truly free clusters is excluded. On the contrary, the influence of He around the RG layers in the experiments of Ref. 8 is most probably negligible. The effect of the He droplet is, indeed, strongly shielded by the RG layers both spatially and energetically. Recall that a typical RG-He bond has a length of about $6-7a_0$ (Ref. 58) and an energy of a few meV,[59] comparable to the metal-RG bonds[60–62] (see column 4 of Table I). However, once coated with the RG layers, the metal cluster lies typically twice farther away from the He droplet than in the case without RG layers, whence a vanishingly small residual interaction between the metal cluster and the He droplet. Thus the relative shifts that we observe by changing the RG material are most probably reliable. Finally, a word of caution is in order. The above-mentioned experimental measurements and our calculations on embedded Na clusters[63] report a broadened, often even fragmented, peak with a width somewhat larger than the shifts we are looking at. The comparison is thus at the edge of experimental and theoretical resolutions.

The data in Table II agree with our theoretical results in that all shifts are very small. Inert environment turns out to be, indeed, inert with respect to the plasmon peak position. Looking in more detail at the relative shifts, one can read for the step from Ne to Ar a redshift of 0.1 eV for Ag_7 in large matrices[55] and of 0.02 eV for Ag_8 in small matrices.[8] The step from Ar to Kr yields 0.06–0.09 eV for Ag_7 in large systems[54] and 0.03 eV for Ag_8 in small systems.[8] The experiments with small RG layers in a He droplet thus yield generally smaller redshifts. This also holds for the step from pure He to Ar environment. This is probably explained by the size of the matrix, as we see from our results in Fig. 3 a slow but steady move toward red (however, systematic errors, by comparing two very different experiments, cannot safely be excluded). Our results for embedded Na clusters, shown in Fig. 3, show a red shift of 0.1–0.2 eV for the step from Ne to Ar and of 0.15–0.2 eV for Ar to Kr, both growing with increasing system size. They confirm all trends seen in experiment, but are generally half an order of magnitude larger. This is probably due to the smaller Wigner-Seitz radius of Ag ($3a_0$ instead of $4a_0$ for Na), which means that Ag structures are much more compact than Na ones and thus couple less strongly to the matrix, because both fill the same RG cavity. This, in turn, produces smaller shifts. In order to check that argument, we have simulated an embedded "Ag_8" cluster simply by rescaling the ionic positions of the Na_8 by the ratio of Wigner-Seitz radii, that is, 3/4, and by reoptimizing the RG positions before the calculations of the optical response of this pseudo Ag_8. We find the same trends as with Na_8 in Fig. 3, but, indeed, reduced by a factor of 3.

Besides, previous theoretical calculations were performed within TDLDA and a jellium model, coupling to the RG materials in terms of a static dielectric medium with dielectric constant ε for different metal clusters, namely, K,[27] Na and Al,[28] and Ag.[29] They always yield redshifts which, moreover, increase with increasing ε. Indeed, the ingredients added in these models can only produce long-range polarization effects and thus can only give a redshift. Our model contains as additional component the RG short-range and repulsive core potentials, which generate a blueshift of the plasmon peak. A clear experimental assessment would yet require a comparison with truly free neutral metal clusters.

V. CONCLUSIONS

We have discussed in this paper static properties and optical response of a small Na cluster embedded in various rare-gas (RG) matrices. For this purpose, we used a recently introduced hierarchical approach combining a fully detailed quantum-mechanical description of the cluster with a classical modeling for the RG environment and its interactions with the cluster. We have studied effects of embedding in RG environment with up to 434 atoms, with particular emphasis on the change with RG material. Various observables were considered. The insertion energy yields stable embedding for Ar and Kr but not for Ne within the considered system sizes. The IP behaves similarly in all three materials: It drops from

free to embedded, and stays nearly constant for all matrix sizes. The electronic and ionic radii of the Na cluster change very little; the most noteworthy effect here is a slight compression of the electron cloud through embedding. Where regard to the optical response is concerned, we studied the effect of the RG matrices on the position of the surface plasmon peak in the metal cluster. The net shift from free to embedded clusters is very small due to a near cancellation of the blueshift from core repulsion with the redshift from dipole polarization in the interaction with the RG atoms. The polarization increases with the RG atomic weight, and thus, final peak position goes from blueshift to redshift on the way from Ne over Ar to Kr. The polarization effect also increases with the size of the RG matrix, which produces a slow and steady trend to red with increasing system size. Comparison with experimental data on embedded Ag clusters confirms these trends and orders of magnitude. Having explored the basic observables of structure and optical response, the way has been opened to applications in truly dynamical scenarios. The large difference in atomic masses of the RG will then play a crucial role and yield interesting effects. Work in that direction is in progress.

ACKNOWLEDGMENTS

This work was supported by the DFG (RE 322/10-1), the CNRS Programme "Matériaux" (CPR-ISMIR), Institut Universitaire de France, and the Humboldt foundation.

[1] *Clusters of Atoms and Molecules 1-Theory, Experiment, and Clusters of Atoms*, edited by H. Haberland, Springer Series in Chemical Physics Vol. 52 (Springer, Berlin, 1994).
[2] *Clusters of Atoms and Molecules 2-Solvation and Chemistry of Free Clusters, and Embedded, Supported and Compressed Clusters*, edited by H. Haberland, Springer Series in Chemical Physics Vol. 56 (Springer, Berlin, 1994).
[3] U. Kreibig and M. Vollmer, *Optical Properties of Metal Clusters*, Springer Series in Materials Science Vol. 25 (Springer, Berlin, 1993).
[4] T. Wenzel, J. Bosbach, A. Goldmann, and F. Träger, Appl. Phys. B: Lasers Opt. **69**, 513 (1999).
[5] T. Wenzel, J. Bosbach, F. Stietz, and F. Träger, Surf. Sci. **432**, 257 (1999).
[6] N. Nilius, N. Ernst, and H.-J. Freund, Phys. Rev. Lett. **84**, 3994 (2000).
[7] M. Gaudry, J. Lermé, E. Cottancin, M. Pellarin, J.-L. Vialle, M. Broyer, B. Prével, M. Treilleux, and P. Mélinon, Phys. Rev. B **64**, 085407 (2001).
[8] T. Diederich, J. Tiggesbäumker, and K. H. Meiwes-Broer, J. Chem. Phys. **116**, 3263 (2002).
[9] J. Chelikowsky, L. Kronik, and I. Vasiliev, J. Phys.: Condens. Matter **15**, R1517 (2003).
[10] M. Marques, A. Castro, G. Bertsch, and A. Rubio, Comput. Phys. Commun. **151**, 60 (2003).
[11] P.-G. Reinhard and E. Suraud, *Introduction to Cluster Dynamics* (Wiley, New York, 2003).
[12] H. Häkkinen and M. Manninen, J. Chem. Phys. **105**, 10565 (1996).
[13] M. Moseler, H. Häkkinen, and U. Landman, Phys. Rev. Lett. **89**, 176103 (2002).
[14] X. Wang, P. Selvam, C. Lv, M. Kubo, and A. Miyamoto, J. Mol. Catal. A: Chem. **220**, 189 (2004).
[15] C. Lv, X. Wang, G. Agalya, M. Koyama, M. Kubo, and A. Miyamoto, Appl. Surf. Sci. **244**, 541 (2005).
[16] X. Wang, Y. Wang, C. Lv, M. Kubo, and A. Miyamoto, Surf. Sci. **601**, 679 (2007).
[17] L. Walewski, P. Bala, M. Elstner, T. Frauenheim, and B. Lesyng, Chem. Phys. Lett. **397**, 451 (2004).
[18] C. Köhler and T. Frauenheim, Surf. Sci. **600**, 453 (2006).
[19] C. Lin, R. Zhang, S. Lee, M. Elstner, T. Frauenheim, and L. Wan, J. Phys. Chem. B **109**, 14183 (2005).
[20] H.-P. Cheng and U. Landman, J. Phys. Chem. **98**, 3527 (1994).
[21] M. Ratner, W. Harbich, and S. Fedrigo, Phys. Rev. B **60**, 11730 (1999).
[22] S. Takami, K. Suzuki, M. Kubo, and A. Miyamoto, J. Nanopart. Res. **3**, 213 (2001).
[23] N. Gresh and D. R. Garmer, J. Comput. Chem. **17**, 1481 (1996).
[24] E. Tapavicza, I. Tavernelli, and U. Rothlisberger, Phys. Rev. Lett. **98**, 023001 (2007).
[25] A. Nasluzov, K. Neyman, U. Birkenheuer, and N. Rösch, J. Chem. Phys. **115**, 8157 (2001).
[26] C. Inntama, L. V. Moskaleva, I. V. Yudanova, K. M. Neymanb, and N. Röscha, Chem. Phys. Lett. **417**, 515 (2006).
[27] A. Rubio and L. Serra, Phys. Rev. B **48**, 18222 (1993).
[28] L. I. Kurkina and O. V. Farberovich, Phys. Rev. B **54**, 14791 (1996).
[29] J. Lermé, B. Palpant, B. Prével, M. Pellarin, M. Treilleux, J. L. Vialle, A. Perez, and M. Broyer, Phys. Rev. Lett. **80**, 5105 (1998).
[30] J. Lermé, Eur. Phys. J. D **10**, 201 (2000).
[31] M. Sulpizi, U. Röhrig, J. Hutter, and U. Rothlisberger, Int. J. Quantum Chem. **101**, 671 (2005).
[32] D. Bucher, S. Raugei, L. Guidoni, M. D. Peraro, U. Rothlisberger, P. Carloni, and M. L. Klein, Biophys. Chem. **124**, 292 (2006).
[33] T. Nakatsukasa, K. Yabana, and G. F. Bertsch, Phys. Rev. A **65**, 032512 (2002).
[34] F. Duplàe and F. Spiegelmann, J. Chem. Phys. **105**, 1492 (1996).
[35] M. Gross and F. Spiegelmann, J. Chem. Phys. **108**, 4148 (1998).
[36] B. Gervais, E. Giglio, E. Jaquet, A. Ipatov, P.-G. Reinhard, and E. Suraud, J. Chem. Phys. **121**, 8466 (2004).
[37] F. Fehrer, P.-G. Reinhard, E. Suraud, E. Giglio, B. Gervais, and A. Ipatov, Appl. Phys. A: Mater. Sci. Process. **82**, 151 (2005).
[38] F. Fehrer, P.-G. Reinhard, and E. Suraud, Appl. Phys. A: Mater. Sci. Process. **82**, 145 (2005).
[39] F. Fehrer, M. Mundt, P.-G. Reinhard, and E. Suraud, Ann. Phys. **14**, 411 (2005).
[40] C. Legrand, E. Suraud, and P.-G. Reinhard, J. Phys. B **35**, 1115 (2002).
[41] S. Kümmel, M. Brack, and P.-G. Reinhard, Eur. Phys. J. D **9**, 149 (1999).
[42] F. Calvayrac, P.-G. Reinhard, E. Suraud, and C. A. Ullrich, Phys.

Rep. **337**, 493 (2000).
[43] G. R. Ahmadi, J. Almlöf, and J. Roegen, Chem. Phys. **199**, 33 (1995).
[44] W. P. Lapatovich, R. Ahmad-Bitar, P. E. Moskowitz, I. Renhorn, R. A. Gottscho, and D. E. Pritchard, J. Chem. Phys. **73**, 5419 (1980).
[45] D. Schwarzhans and D. Zimmermann, Eur. Phys. J. D **22**, 193 (2003).
[46] R. Brühl, J. Kapetanakis, and D. Zimmermann, J. Chem. Phys. **94**, 5865 (1991).
[47] B. Montag and P.-G. Reinhard, Phys. Lett. A **193**, 380 (1994).
[48] B. Montag and P.-G. Reinhard, Z. Phys. D: At., Mol. Clusters **33**, 265 (1995).
[49] F. Calvayrac, P.-G. Reinhard, and E. Suraud, Phys. Rev. B **52**, R17056 (1995).
[50] F. Calvayrac, P.-G. Reinhard, and E. Suraud, Ann. Phys. (N.Y.) **255**, 125 (1997).
[51] K. Yabana and G. F. Bertsch, Phys. Rev. B **54**, 4484 (1996).
[52] F. Fehrer, Ph.D. thesis, 2006.
[53] C. Félix, C. Sieber, W. Harbich, J. Buttet, I. Rabin, W. Schulze, and G. Ertl, Phys. Rev. Lett. **86**, 2992 (2001).
[54] S. Fedrigo, W. Harbich, and J. Buttet, Phys. Rev. B **47**, 10706 (1993).
[55] F. Conus, V. Rodrigues, S. Lecoultre, A. Rydlo, and C. Félix, J. Chem. Phys. **125**, 024511 (2006).
[56] T. Kinoshita, K. Fukuda, Y. Takahashi, and T. Yabuzaki, Phys. Rev. A **52**, 2707 (1995).
[57] T. Kinoshita, K. Fukuda, and T. Yabuzaki, Phys. Rev. B **54**, 6600 (1996).
[58] K. P. Huber and G. Herzberg, *Constants of Diatomic Molecules*, Molecular Spectra and Molecular Structure Vol. IV (Van Nostrand-Reinhold, New York, 1979).
[59] K. T. Tang and J. P. Toennies, Z. Phys. D: At., Mol. Clusters **1**, 91 (1986).
[60] F. Ancilotto and F. Tagio, Z. Phys. B: Condens. Matter **98**, 309 (1995).
[61] Z. J. Jakubek and M. Takami, Chem. Phys. Lett. **265**, 653 (1997).
[62] M. Mella, M. C. Colombo, and G. Morosi, J. Chem. Phys. **117**, 9695 (2002).
[63] F. Fehrer, Ph.D. thesis, Universität Erlangen/Nürnberg, 2006.